RESEARCH ARTICLE

Adsorption removal and photocatalytic degradation of azithromycin from aqueous solution using PAC/Fe/Ag/Zn nanocomposite

Azadeh Mehrdoost[1] · Reza Jalilzadeh Yengejeh[1] · Mohammad Kazem Mohammadi[2] · Azadeh Haghighatzadeh[3] · Ali Akbar Babaei[1,4,5]

Abstract
The improper use of antibiotics and their discharge into the environment can have serious and hazardous consequences. The purpose of this research is to synthesize an activated carbon impregnated magnetite composite (PAC/Fe), prepare PAC/Fe/Ag/Zn nanocomposites, and innovate by simultaneously synthesizing two metals, zinc and silver, on magnetically activated carbon and check its ability to remove azithromycin antibiotic (AZT) from an aqueous solution via UV system. PAC/Fe/Ag/Zn nanocomposites were characterized by various techniques including XRD, FESEM, and EDX. A series of batch experiments were carried out under various experimental conditions such as pH of the solution (3–11), contact time (0–120 min), initial concentration of AZT (10–40 ppm), amount of PAC/Fe/Ag/Zn nano-absorbent (0.01–0.04 g/l), and recoverability and reuse. Some common isotherm models were used for the study of AZT adsorption removal and finding the best model. Also, kinetic studies of AZT removal were performed by fitting the experimental data on first-order and second-order models. In this system, under optimal conditions of pH = 9, 120 min with 0.04 g/l of PAC/Fe/Ag/Zn, 99.5% of 10 ppm AZT were degraded under UV-C irradiation. Furthermore, the obtained results of isotherm and kinetic studies revealed that Langmuir ($R^2 = 0.9336$) isotherm model, and the pseudo-first-order kinetic model ($R^2 = 0.9826$) had the highest correlation with the experimental data of AZT antibiotic adsorption. Finally, the reusability experiments showed that PAC/Fe/Ag/Zn nanocomposites have a high ability of antibiotic adsorption and high stability after four cycles of application (99.5 to 40%).

Keywords PAC/Fe/Ag/Zn · Nanocomposite · Azithromycin · Adsorption · Antibiotic removal · Synthesis

Responsible Editor: Sami Rtimi.

Highlights PAC/Fe/Ag/Zn nanocomposite has been synthesized and characterized as a new absorbent.

Efficient AZT adsorption removal by PAC/Fe/Ag/Zn Nanocomposite was found 99.5% at pH = 9.

The adsorption kinetics and adsorption isotherms of AZT were fitted with the pseudo-first-order model and the Langmuir model.

✉ Reza Jalilzadeh Yengejeh
   r.jalilzadeh@iauahvaz.ac.ir

[1] Department of Environmental Engineering, Ahvaz Branch, Islamic Azad University, Ahvaz, Iran

[2] Department of Chemistry, Ahvaz Branch, Islamic Azad University, Ahvaz, Iran

[3] Department of Physics, Ahvaz Branch, Islamic Azad University, Ahvaz, Iran

[4] Environmental Technologies Research Center, Ahvaz Jundishapur University of Medical Sciences, Ahvaz, Iran

[5] Department of Environmental Health Engineering, School of Public Health, Ahvaz Jundishapur University of Medical Sciences, Ahvaz, Iran

Introduction

Pharmaceutical pollutants are one of the essential pollutants for water resources, the health and environmental effects of which have been thoroughly estimated (El Bekkali et al. 2018). Among pharmaceuticals, antibiotics have received special attention because they are biologically active and induce bacterial resistance, even in small amounts, through constant exposure. This has become a more important issue because they are difficult to remove (Ghosh et al. 2016) (Huízar-Félix et al. 2019). About 30 to 90% of antibiotics are excreted unchanged in the body of humans and animals as active compounds in urine and feces (Liu et al. 2019).

Antibiotics are divided into major categories: macrolides, tetracyclines, and chloramphenicol. AZT is one of the macrolide antibiotics used as a broad-spectrum antimicrobial agent to treat infectious diseases in humans and animals (Naraginti et al. 2019). There are many ways to release antibiotics into the environment, but in general, conventional

water and wastewater treatment processes are not able to remove these compounds.

Up to the present, various physical, chemical, and biological treatment methods have been suggested to remove antibiotics from the aquatic environment, such as flocculation (Jia et al. 2016), coagulation (Choi et al. 2008), air striping (Verklin and Mandell 1977), catalytic process (Cheng et al. 2021), membrane process (Xu et al. 2019), ultrafiltration (Ren et al. 2018), electrochemical treatment (Ahmadzadeh and Dolatabadi 2018), ultrasonic cavitation (Wang et al. 2013), biological filtration (Chen et al. 2017), biological membrane (Dorival-Garcia et al. 2013), reverse osmosis (Košutićb et al. 2007), photocatalytic process degradation (Beltran et al. 2008), advanced oxidation (Belghadr et al. 2015), electro degradation (Foroughi et al. 2017), and adsorption removal (Mehrdoost et al. 2021).

Despite their advantages, these methods have several drawbacks, which in most cases make them difficult to be adopted. For physical methods such as coagulation and centrifuge, a secondary pollutant is usually produced. In biological methods, the large amount of time required for the low efficiency of the process becomes problematic (Gashtasbi et al. 2018). In the surface adsorption removal method, pollutants are collected and removed from the environment, but only those from the liquid phase transfer to a solid phase (Gashtasbi et al. 2017).

Among the abovementioned methods, the adsorption removal method has several advantages such as ease of application, low cost, high efficiency, and risk-free process. That is why adsorption is one of the best ways to remove antibiotics (Hou et al. 2020). Adsorption removal efficiency depends on the type of the adsorbent and the properties of the adsorbent including surface area, porosity, and pore (Mahmoud et al. 2020). Various materials have been repeatedly used as adsorbents to remove antibiotics from aquatic environments such as carbon (Chowdhury et al. 2021), mineral (Zhu et al. 2020), polymeric resins (Dutta et al. 1999), metals, and their oxides (Bayati et al. 2021), gel chitosan (Yaqubi et al. 2021), zeolites (Chen et al. 2019), ceramics (Gao et al. 2020), etc.

While the removal of antibiotics via adsorbents has been investigated extensively, the adsorption removal of the antibiotic AZT using PAC/Fe/Ag/Zn is not adequately studied. Therefore, the main objectives of this study are to prepare a magnetic nanocomposite impregnated with activated carbon, synthesize zinc and silver metals on it and its application to remove the antibiotic AZT from aqueous solution, and investigate the effect of various experimental variables on the removal efficiency. In addition, adsorption isotherms and adsorption kinetics were studied to find the most suitable models with experimental data. Finally, adsorption and desorption tests were performed to evaluate the performance of PAC/Fe/Ag/Zn nano-adsorbent after several cycles.

Materials and methods

Materials

Ferrous sulfate heptahydrate ($FeSO_4·7H_2o$), sodium borohydride ($NaBH4$), zinc nitrate hexahydrate ($Zn(NO_3)_26H_2O$), trisodium citrate dehydrate ($C_6H_9Na_3O_9$), and tetraethyl orthosilicate (TEOS) were prepared by Sigma-Aldrich Company. Other reagents and solvents like NaOH, HCL, methanol, ethanol, PAC, and $AgNO_3$ were purchased from Merc company (Darmstadt, Germany). AZT was taken from Merc company. In addition, shaker equipment (Vibramax 100 Heidolph), Spectrometer (T90 + UV/VIS), UV lamp (T5 fluorescent tube — 6w 230v cooling light), pH meter (Inolab- Sentix 41), and ultrasonic device (PARASONIC 7500,220 VAC, Iran) were applied in experiments.
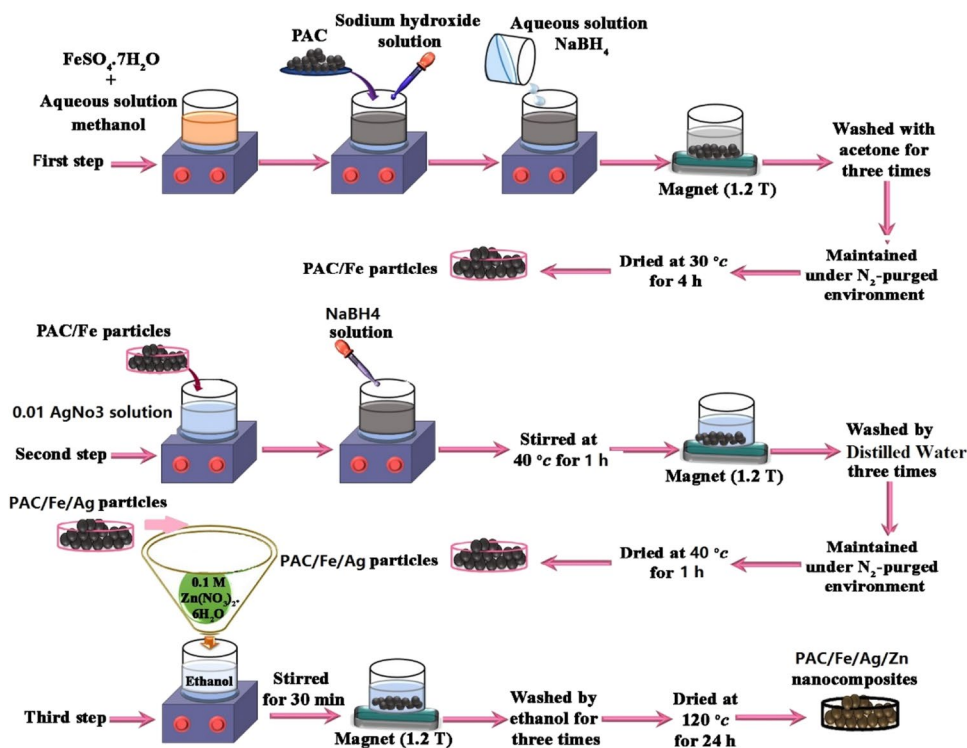
Synthesis

Synthesis of PAC/Fe

Initially, in a 250-ml balloon, 5 g $FeSO_4·7H_2O$ in 200 ml of methanol-distilled water solution at a ratio of 30:70 v/v was added, and then the solution was stirred for 30 min. Next, 5 g PAC (active carbon) was added to the mixture. The mixture pH was adjusted at 7 by adding 3.8 M NaOH to the solution. It was observed that many small bubbles on the surface of the solution were coming out of the mixture. The mixture was stirred for an hour to remove the bubbles. Afterward, using a 1.2 T magnet, the formed magnetic precipitate was collected, and subsequently, the excess water was removed from the balloon. The resulting precipitate was washed several times (3 to 4 times) using acetone, then exposed for 3 h to N2-purged environment at a temperature of 40 °C and dried at 30 °C for an hour using a rotary (Fig. 1) (Kakavandi et al. 2014a, b).

Synthesis PAC/ Fe/Ag

In this step, 2.5 g of the previously synthesized material (PAC/Fe) was added to a diluted solution of AgNO3 (0.01 M), and then, the mixture was placed in an oil bath at 200 °C temperature. After that, it was vigorously stirred for 1 h. Finally, a 3 M solution of NaBH4 was prepared and added to the previous solution, and the previous mixture was stirred until the bubbles were completely removed. Subsequently, by using a 1.2 T magnet, a magnetic nanoparticle was collected, and finally, the resulting nanoparticle was washed several times with distilled water. Later, it was exposed for an hour by using a rotary and for 3 h

to N2-purged environment at 40 °C temperature (Fig. 1) (Kakavandi et al. 2014a, b).

Synthesis PAC/Fe/Ag/Zn

Initially, 1.5 g of the nanoparticles synthesized in the previous step was dissolved in 50 ml ethanol solution (99%), and then 50 ml of 0.1 M Zn (NO$_3$)26H$_2$O solution was added. The mixture was stirred for 30 min, and nanoparticles were collected by a 1.2 T magnet and washed several times using ethanol. In the next step, they were exposed to an N2 purged environment and dried for 24 h at 120 °C temperature in a hot air oven (Fig. 1) (Gautam et al. 2015).

Characterization of the synthesized absorbent

To study topographical and elemental information, the microscopic feature of nanocomposites was investigated with field emission scanning electron microscopy (FESEM, ZEISS company, Sigma VP model) (Velliyan and Rajendran 2021), crystallographic structure analysis was carried out by X-ray diffraction (XRD, x petro pro equipment, Panalytical company) (Sundaram et al. 2020), an energy dispersive X-ray analyze (EDX) was used to provide elemental identification (Ech-Chihbi et al. 2020), and diffuse reflection spectroscopy (DRS) was carried out.

Batch experiment

This study was performed discontinuously to remove AZT antibiotics by PAC/Fe/Ag/Zn nano-adsorbents in 500-mL containers containing 250-mL samples in a laboratory at room temperature (25 °C ± 1).

The effect of pH parameters (3–11), contact time (120 min), initial concentration of AZT (10–40 ppm), the amount of PAC/Fe/Ag/Zn nano-absorbent (0.01–0.04 g/l), recoverability, and reuse were also investigated. In each step, by keeping all variables constant and changing only one variable, the optimal value for the desired parameter was determined. All test steps were repeated three times to reduce the error rate. To prevent any errors, all used sampling containers were washed with acid and finally rinsed with distilled water. Hydrogen chloride acid and sodium hydroxide base were used to adjust the pH in the study.

To prepare the stock solution of AZT, 100 mg AZT was dissolved in 40 mL methanol using ultrasonic and made 100 mL by using distilled water. In the next step, using this solution, the desired concentration was made at the volume of 250 mL.

In the reduction step, nanoparticle precipitate was collected in the adsorbent optimization step and used again to remove the AZT. After the experiments, the value of antibiotic removal efficiency along with its adsorption capacity was calculated and analyzed using Eqs. 1 and 2:

$$D(\%) = \frac{(C_0 - C_t)}{C_0} \times 100 \tag{1}$$

$$q_e = \frac{(C_0 - C_e)V}{m} \tag{2}$$

The D is the removal efficiency of the AZT in percentage; C_0 and C_e are the primary and secondary concentration of the AZT in mg and L, respectively; m is the absorbent mass in g; and V is the volume of solution in L (Amin et al. 2021). All statistical data obtained from this study were analyzed using Excel statistical software, and the relevant graphs were extracted. Finally, the data were fitted with adsorption kinetic and isotherm models.

Kinetic

Studying the kinetics of the adsorption removal process is essential to investigate the factors affecting the reaction rate (Bachmann et al. 2020) (Salari 2019). The two most important models widely used in sources for the adsorption removal process are the pseudo-first kinetic model and pseudo-second kinetic model (Sohrabi et al. 2021). Therefore, in this study, these models were used to describe the data obtained by UV-spectroscopy, and the diagrams of these models were drawn.

Equations 3 and 4 represent the pseudo-first kinetic model and pseudo-second kinetic model, respectively.

$$-1\ln\left(\frac{C_t}{C_0}\right) = k_1 t \tag{3}$$

$$\left(\frac{1}{C_t} - \frac{1}{C_0}\right) = k_2 t \tag{4}$$

where parameters of k_1 and k_2 are the reaction rate constants of first- and second-order models in min^{-1} and L mg^{-1} min^{-1}, respectively (Babas et al. 2021).

Isotherm

Adsorption isotherms are used to explain the reaction between the absorbate material and adsorbents (Khan and Khan 2018). Isotherms also express the adsorption capacity of an adsorbent (Nnadozie and Ajibade 2021). In the present study, to investigate the empirical data analysis and to describe the adsorption equilibrium state between solid and liquid phases, the Langmuir (Eq. 5) and Freundlich (Eq. 6) isotherm models were applied. For the Langmuir adsorption model, a continuous monolayer of adsorbate molecules surrounding a homogeneous solid surface is the conceptual basis (Ghaedi et al. 2015), while the experimental equation

of the Freundlich isotherm is based on the adsorption multilayer, non-uniform, and non-heterogeneous absorbed material on absorbent (Alalwan et al. 2021).

The linear form of Langmuir and Freundlich isotherm model is described below Eqs. 5 and 6. where K_L is the Langmuir constant (L mg^{-1}), K_f the Freundlich constant, q_{max} maximum adsorption capacity (mgg^{-1}), n_f the heterogeneity factor, c_0 initial AZT concentration, q_e the amount of AZT absorbed at equilibrium, and C_e, equilibrium concentration of AZT. The knowledge of the favorability and unfavorability of the adsorption removal process can be described by the dimensionless constant R_L. Equation 7 represents the value of R_L, if $R_L > 1$ undesirable adsorption, $0 < R_L < 1$ desirable adsorption, $R_L = 1$ linear adsorption and $R_L = 0$ irreversible adsorption (Arabpour et al. 2021). To determine the nonlinear regression analysis, Microsoft Excel was applied:

$$\frac{C_e}{q_e} = \frac{1}{q_{max}K_L} + \frac{C_e}{q_{max}} \tag{5}$$

$$\log q_e = \log K_F + \frac{1}{n_F}\log C_e \tag{6}$$

$$R_L = \frac{1}{1 + K_L C_0} \tag{7}$$

Ability to reuse PAC/Fe/Ag/Zn nano-adsorbents to remove AZT antibiotic

To evaluate the recoverability and reuse of synthesized nano-adsorbents in the removal of AZT antibiotics, the sequential adsorption removal and desorption cycles by using methanol as the adsorbent, in an optimal adsorbent dosage, optimal initial antibiotic concentration, optimal pH, and optimal contact time were examined. The resulting sediment was collected in the optimization stage and used again to remove antibiotics. At each stage, the amounts of adsorption and desorption were calculated and compared with the previous steps.

Results and discussion

Characterization of the obtained PAC/Fe/Ag/Zn

An X-ray diffraction test was used to characterize the synthesized sample (Salari et al. 2021). The X-ray diffraction pattern of nanoscale PAC/Fe/Ag/Zn structure in wavelength range 2θ from 20 to 80 is shown in Fig. 2. The diffraction pattern of Zn nanostructures shows three scatter peaks in positions 36/05°, 39/22°, and 43/54°,
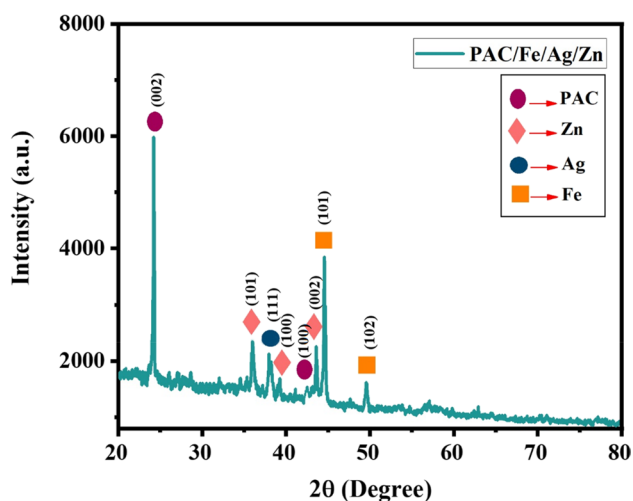
Fig. 2 XRD patterns of PAC/Fe/Ag/Zn

respectively, corresponding to the (101), (100), and (002) reflective plates, which according to the reference card 00–001-1224 confirms the formation of a hexagonal crystal structure for the Zn structure (Gautam et al. 2015) (Qin et al. 2017).

The peaks in position 44/53° and 49/52° according to the reference card 00–050-1275 are related to the Fe structure in the hexagonal phase, and the reflective pages for these peaks are (101) and (102), respectively. The peaks that appear in positions 24/12° and 42/47° are related to the PAC structure in the synthesized nanostructure, and

the reflective plates of these peaks are (002) and (100), respectively (Kakavandi et al. 2014a, b) (Gautam et al. 2015) (Qin et al. 2017).

Also, according to the reference card 00–001-1164, the peak in position 37/92° belongs to the silver in the cubic phase, and the reflective page (111) corresponds to the peak (Kakavandi et al. 2014a, b).

To study the morphology of the synthesized nanostructures, a field-based scanning electron microscopy test (FESEM) was used (Salari et al. 2018). Figure 3 shows the FESEM images of the PAC/Fe/Ag/Zn nanostructures at 200-nm magnification. As it can be seen in Fig. 3a, the synthesized nanostructures have two different morphologies. Many nanoparticles have a nanowire structure, and a small number have nanocrystals. According to Fig. 3b, it can be said that nanowires have a diameter of 27 to 66 nm.

To study how constituent elements are distributed on the surface of synthesized nanostructures, an elemental mapping test was applied using field scanning electron microscopy. Figure 3c shows the selected range for elemental mapping analysis. Figure 3d shows the distribution of nanocomposite elements in the PAC/Fe/Ag/Zn nanostructures. According to Fig. 3, the elements silver, activated carbon, zinc, and iron are evenly distributed on the nanostructured surface, and the elements are well dispersed.

To quantitatively study the constituent elements of the synthesized nanostructures, the scattered element X-ray diffraction test was used (Salari 2020). Figure 4 shows the EDX spectrum, and Table 1 shows quantitative corresponding results for PAC/Fe/Ag/Zn nanostructures. As can be seen,

Fig. 3 FESEM Image of the PAC/Fe/Ag/Zn nanostructures: **a** morphologies of nanostructure, **b** size of nanostructures, **c** selected range for elemental mapping analysis, **d** distribution of nanocomposite elements in nanostructures
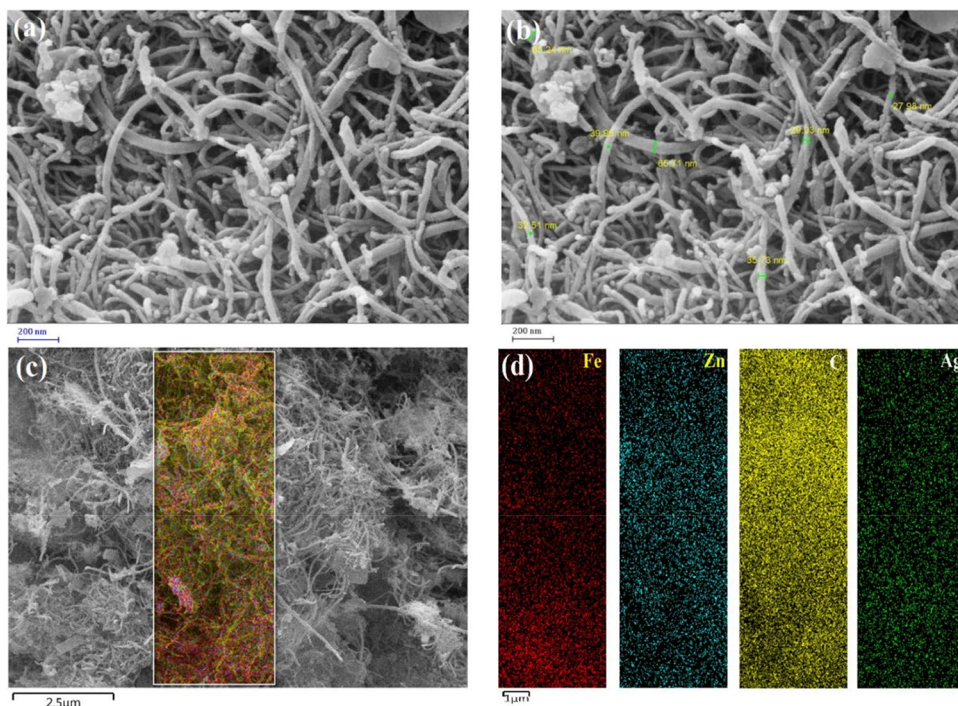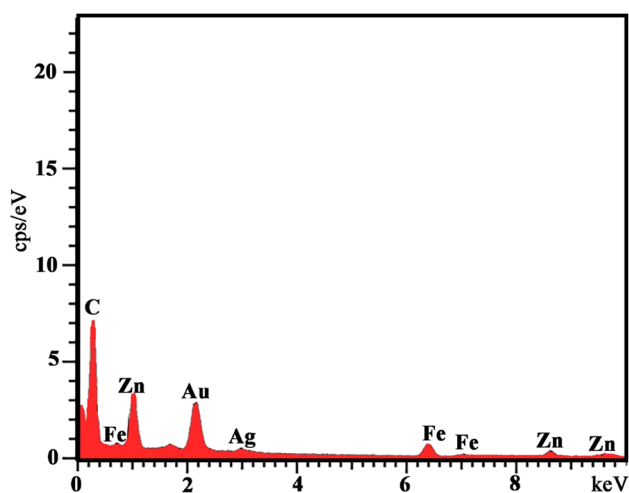
Fig. 4 EDX spectrum

Table 1 Quantitative distribution of nanocomposite elements in nanostructures

Ag (wt. %)	Zn (wt. %)	Fe (wt. %)	C (wt. %)	Element
3.2	21.1	18.8	56.9	PAC/Fe/Ag/Zn

there is no other element in the EDX spectrum other than the constituent elements of PAC/Fe/Ag/Zn nanostructures. The Au peak observed in Fig. 4 is related to the nanostructured substrate when preparing the sample for EDX analysis.

Diffuse reflection spectroscopy (DRS) UV–Vis was used to investigate the absorption optical properties of PAC/Fe/Ag/Zn nanocomposite. Figure 5a shows the UV–Vis absorption spectra of PAC/Fe/Ag/Zn nanocomposite in the wavelength range from 200 to 800 nm. According to Fig. 5, the PAC/Fe/Ag/Zn nanocomposite shows a wide absorption in the UV region at wavelengths of about 303 and 364 nm. Previous studies have reported that due to surface plasmon

resonance (SPR), silver metal absorbs light at wavelengths of about 317 and 375 nm, which is related to the mass oscillation of conducting electrons exposed to external electromagnetic fields (Zhang et al. 2016a, b) (Liu et al.2018). The results from Fig. 5a explain that loading silver onto the surface of PAC/Fe/Ag/Zn nanocomposites can increase the ability to absorb light by extending the amplitude of the light response to larger wavelengths. There are several methods for estimating the optical band gap energy of semiconductors, one of the most famous of which is the Tauc/David-Matt models explained according to Eq. 8:

$$(Ahv) = a(hv - E_g)^{n/2} \tag{8}$$

where a is absorption coefficient, h is plank's constant, v is light frequency, E_g is semiconductor band gap, and A is a constant. The value of n is dependent on transition type and directly/indirectly allows transition ($n = 1$ for direct transition and $n = 4$ for indirect transition). Figure 5b shows the PAC/Fe/Ag/Zn energy gap by drawing the plot of $(ahv)^2$ versus hv. The band gap of PAC/Fe/Ag/Zn appeared at about 3.44 eV (Salari et al. 2018).

Photocatalytic degradation properties of PAC/Fe/Ag/Zn for AZT

Effects of pH on removal of AZT by nano-absorbent PAC/Fe/Ag/Zn

pH is one of the most important parameters affecting the efficiency of pollutant removal in wastewater. pH affects adsorption capacity, the degradation of the target compound, the distribution of electrical charge on the photocatalyst, and the oxidation of the capacity band. Previous studies also show that pH plays an important role in the removal of antibiotics (Hussain et al. 2021) (Kavitha et al. 2021) (Salari 2021). In this study, the effect of solution pH in the removal

Fig. 5 DRS pattern of PAC/Fe/Ag/Zn: **a** adsorption spectra, **b** band gap energy
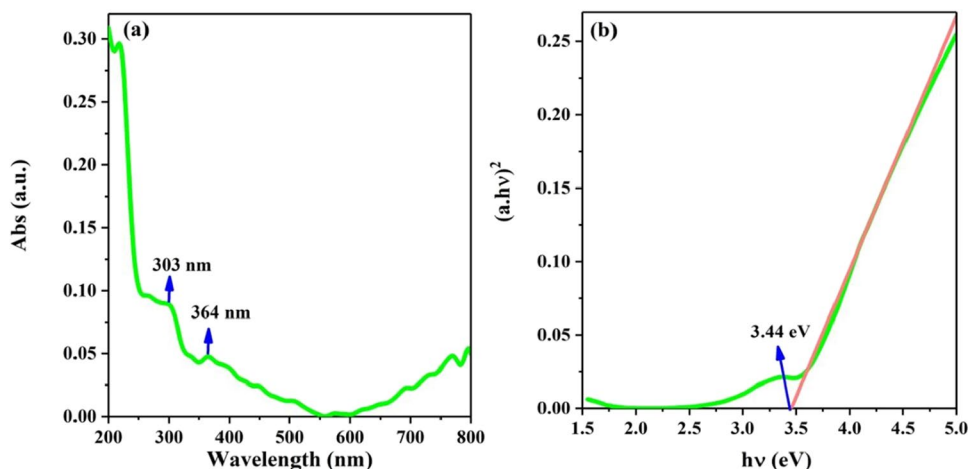
of AZT by nano-adsorbents PAC/Fe/Ag/Zn was investigated in a range of 3 to 11 (in 4 levels 3, 7, 9, and 11) in the initial concentration of AZT 10 mg/L, adsorbent dosage 0.04 g/L, and contact time 120 min were used for all solution. The results of the pH effect on the removal efficiency are shown in Fig. 6a. As shown in Fig. 6a, by increasing pH values, the removal efficiency was increased. This showed that the most removal percentage was 80% at pH = 9, and the lowest removal percentage was 33.3% at pH = 3. Thus, pH = 9 was chosen as the optimal pH.

The findings of Wang et al. (2020) showed that the optimal pHs for the removal adsorption of tetracycline (TC), ciprofloxacin (CIP), and sulfadiazine (SDZ) from aqueous solutions using glucose-based mesoporous carbon (GMC) were 6, 6, and 4, respectively.

Sayadi et al. (2019) reported that the photocatalytic degradation of AZT in the aqueous environment by GO@Fe_3O_4/ZnO/SnO_2 nanocomposite under optimal conditions of pH = 3, 120 min with 1 g/L of GO@Fe_3O_4/ZnO/SnO_2, 90.06% of 30 mg/L AZT was degraded under UV-C irradiation.

In explaining these findings, the predominant surface electric charge of materials in the natural state may be positive or negative, depending on the surface properties, especially the functional groups and components of the material (Kanani et al. 2019). PAC/Fe/Ag/Zn nano-adsorbents have acidic properties due to their metal groups Fe, Zn, and Ag. The antibiotic AZT has alkaline properties due to having alkaline groups in its composition such as Z, O, OH. At neutral pH, free electrons of alkaline groups on the surface of AZT react with the empty orbitals in the nano-adsorbent metal groups PAC/Fe/Ag/Zn by forming a dative bond. Thus, AZT is absorbed on the adsorbent surface. In acidic environments where the pH is less than 7, the base groups are proteinaceous on the surface of AZT and lose their ability to form dative bonds with nano-adsorbent metal groups. As a result, the adsorption removal of antibiotics by the adsorbent reduces. However, in alkaline environments with a pH greater than 7, the alkaline groups on the surface of AZT are more inclined to form a dative bond with the metal groups in nano-adsorbents due to the high density of negative charge on them. Therefore, with increasing pH, the adsorption removal of AZT by PAC/Fe/Ag/Zn nano-adsorbents increases.

Effect of contact time on the removal of AZT by nano-adsorbent PAC/Fe/Ag/Zn

The effect of reaction time was also investigated as a variable (Pirsaheb et al. 2019). The AZT elimination experiments were tested over 120 min and in times of 20, 40, 60, 80, 100, and 120 min. Figure 6b illustrates AZT adsorption removal

Fig. 6 Experimental parameter effects on AZT adsorption onto PAC/Fe/Ag/Zn: **a** pH, **b** contact time, **c** absorbent, **d** dosage and initial concentration of AZT
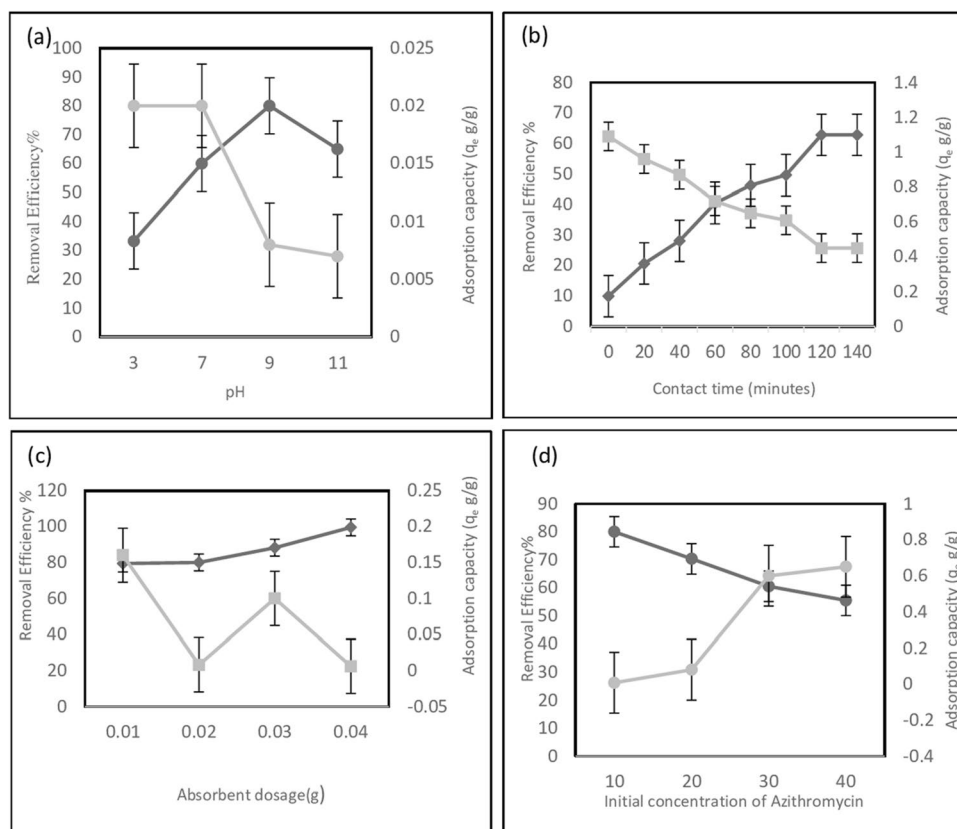
during 120 min. As evidenced in Fig. 6b, by the increase in contact time up to 120 min, the removal efficiency of AZT increased, and after about 120 min, the removal of AZT was not done. Thus, the contact time of 120 min was chosen as the optimal contact time.

In the present study, the amount of adsorption removal of AZT was increased by increasing contact time. This is due to the increase in the probability of the collision of AZT molecules with the adsorptive surface.

Similar results by using the photocatalytic degradation process under visible light for the tetracycline antibiotic removal were obtained whereby as the contact time increases, the adsorption removal efficiency of tetracycline increases as well (Galedari et al. 2019). Furthermore, the optimal reaction time for adsorptive removal of 28 antibiotics using activated carbon was reported as 120 min (Zhang et al. 2016a, b).

According to the findings, it can also be stated that the process of AZT adsorptive removal on PAC/Fe/Ag/Zn nano-adsorbents occurs in two consecutive stages; the adsorption of AZT in the thin layer, which is the first stage of adsorption, occurs faster, but the next stage of the adsorption process in the porous region, which leads to increased adsorption inside the adsorbent, is delayed. In the first step, which is faster, the AZT molecules are transferred from the liquid phase to the outer surface of the PAC/Fe/Ag/Zn nano-adsorbent. In the second stage, when the transfer rate is lower, the diffusion of AZT molecules occurs between the pores of PAC/Fe/Ag/Zn nano-adsorbents. During contact time after 120 min, there are almost no significant changes in the number of the removed antibiotics. This can cause the surface pores of PAC/Fe/Ag/Zn nano-adsorbents to fill and prevent antibiotic and adsorbent reactions.

The adsorption removal of the AZT in the first few minutes was very fast, and over time, the speed of adsorption removal decreased. This could be attributed to the reduction of the dissolved AZT concentration and the reduction of active points on the adsorbent surface. The results showed the adsorption removal of AZT in the thin layer, which is the first stage of adsorption, will happen faster, but the next stage of the adsorption process in the porous zone, which results in increasing adsorption inside the adsorbent, happens with delay as what was found in the previous study (Elessawy et al. 2020).

Effect of adsorbent dosage

Absorbent dosage was investigated as one of the variables affecting the adsorption capacity in the batch experiment. The effect of absorbent initial dosage on removal efficiency is shown in Fig. 6c, and a direct relationship between the adsorbent dosage and AZT adsorptive removal was observed. As shown in Fig. 6c, by increasing the amount of absorbent, the removal efficiency has also increased. By increasing the adsorption dosage from 0.01 to 0.04 g/L, the efficiency of AZT adsorption removal increases from 79.4 to 99.5%. However, with increasing adsorption dosage from 0.04 g/L to above, there is no change in the AZT removal efficiency.

The finding of Kakavandi et al. (2014a, b) shows that by increasing magnetic activated carbon dosage from 1 to 5 g/L, the removal efficiency of amoxicillin antibiotics has increased.

The results showed that the efficiency of AZT adsorption removal increases by increasing the amount of the absorbent. Increasing the amount of the absorbent will increase the efficiency of AZT removal due to the specific and inner pores of the absorbent. Although by increasing the amount of adsorbent dosage, the removal efficiency increases, the amount of absorbed AZT is reduced per gram of the adsorbent. In fact, with increasing adsorbent dosage, the total capacity of active points on the absorbent surface has not been fully utilized, and this has reduced the amount of the AZT adsorption removal in the absorbent mass unit. The increase in adsorption removal percentage, in this case, is due to the increase in the adsorbent surface and the consequent increase in the access of antibiotic molecules to the adsorption sites on the PAC/Fe/Ag/Zn nano-adsorbent and the constant number of antibiotic molecules. Also, the decrease in adsorption capacity can be due to the lack of antibiotic concentration in higher amounts of adsorbent in the environment and the unsaturation of adsorbent sites due to increased adsorbent relative to antibiotics in adsorption reactions. Similar results have been reported by previous researchers (Mohammed and Kareem 2019).

Effects of initial concentration AZT

The effect of the initial concentration of AZT on adsorption removal efficiency and adsorption capacity is shown in Fig. 6d. As shown in Fig. 5d, by increasing the initial concentration of AZT from 10 to 40 mg/L, removal efficiency was reduced from 80 to 55.47%. This result indicates that increasing the initial concentration of AZT has a negative effect on removal efficiency. It means, with increasing the initial concentration of AZT, the adsorption removal efficiency is reduced, which is normal because with increasing the initial AZT concentration, the number of adsorption sites remains constant compared to the increase in the number of molecules of the adsorbed substance, and the adsorbent surface is saturated at high antibiotic concentrations, in regard to which similar results have been observed in previous studies (Nasseh et al. 2019). The results of the present study showed that increasing the initial concentration of AZT has a positive effect on the adsorption capacity, so that with increasing the initial concentration of AZT from 10 to

40 in the concentration of 0.04 g/l adsorbent, the adsorption capacity increased from 0.008 to 0.65. This is because of the increased likelihood of contact between the adsorbent and antibiotic.

Findings from the studies of Samarghandi et al. (2015) on the removal of cephalexin using zeolite and zeolite-stabilized manganese oxide nano-adsorbent showed that by increasing concentration of cephalexin from 10 to 40 mg/L, the cephalexin adsorption removal efficiency was decreased.

Kinetic and isotherm studies

In this study, the kinetics of AZT adsorption removal on PAC/Fe/Ag/Zn nano-adsorbent were calculated using fitting experimental data with two kinetic models: pseudo-first-order and pseudo-second-order models at different initial concentrations of AZT. The $\ln(q_e - q_t)$ is plotted over time for the pseudo-first-order model in Fig. 7a, and the values of q and k are calculated from the values of the slope and intercept of the graph, respectively. Also, diagram t/q over t is plotted for pseudo-second-order in Fig. 7b, and the values of q and k are calculated from the slope and intercept of the graph, respectively.

The obtained kinetic parameters and coefficients of correlation are summarized in Table 2. According to Table 2, the correlation coefficient in the pseudo-first-order kinetic model was higher than the pseudo-second-order model and was approximately equal to 1(0.9826). Therefore, the adsorption removal process follows the pseudo-first-order kinetic model, and the experimental data obtained from AZT adsorption removal experiments are consistent with the pseudo-first-order kinetic model, and the data is better described by this model.

The results of Sharma et al. (2020) for the photocatalytic mineralization of ofloxacin antibiotic in the aqueous solution using graphene oxide supported mesoporous zinc oxide (rGO@ZnO) showing that removal antibiotic followed from the pseudo-first-order kinetic model.

Table 2 Kinetic adsorption coefficients for removal AZT using PAC/Fe/Ag/Zn nano-adsorbent

Value				Parameter	Model
Initial antibiotic concentrations (ppm)					
40	30	20	10		
0.01543	0.05211	0.01021	0.01363	K_1	Pseudo-first order
0.99061	0.97122	0.98668	0.9826	R_1^2	
0.00659	0.00718	0.0696	0.7782	K_2	Pseudo-second order
0.98926	0.95197	0.9834	0.9519	R_2^2	

Therefore, the findings reveal that the dominant mechanism in the antibiotic adsorption removal process on the PAC/Fe/Ag/Zn nano-adsorbent is physical adsorption, and surface adsorption occurs by penetration into a layer or boundary. In fact, in cases where adsorption occurs from within a layer (boundary), the equilibrium data follow pseudo-first-order kinetics and in situations where chemical adsorption controls the process, the equilibrium data follow pseudo-second-order (Anirudhan and Deepa 2017).

Adsorption isotherms are one of the most influential factors in the design of adsorption systems (Gholamiyan et al. 2020). Therefore, the experimental data of AZT on nano-adsorbent PAC/Fe/Ag/Zn were fitted using two models of isotherm Langmuir and Freundlich. The linear Langmuir diagram is plotted in Fig. 8a, and the values of K_L and q_e are calculated from the values of the slope and intercept of the graph, respectively. Also, the linear Freundlich diagram is plotted in Fig. 8b, and the values of K_f and n_f are calculated from the slope and intercept of the graph, respectively.

The results obtained from the adsorption removal parameters related to Langmuir and Freundlich equation are summarized in Table 3 that illustrates the obtained constants and the related coefficients of the correlation of each applied model. The compatibility of experimental data with the isothermal models of Langmuir and Freundlich was investigated using a correlation coefficient.

Fig. 7 Time-dependent adsorption removal efficiency of PAC/Fe/Ag/Zn for AZT corresponding: **a** pseudo first-order, **b** pseudo second-order kinetic models
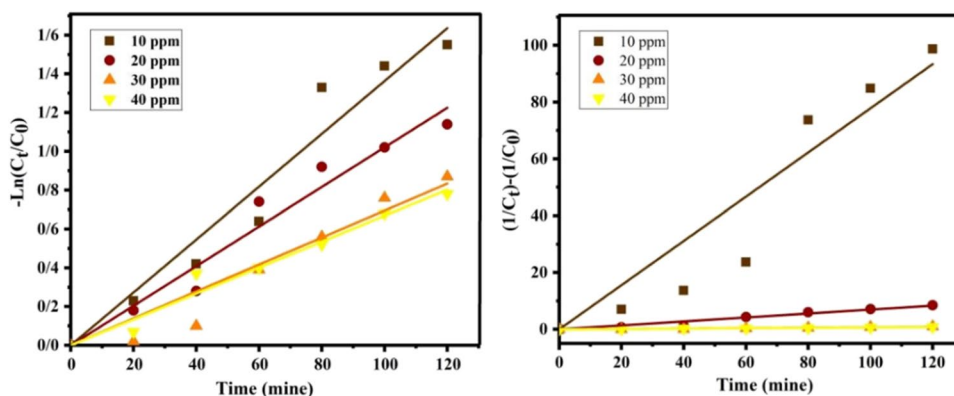
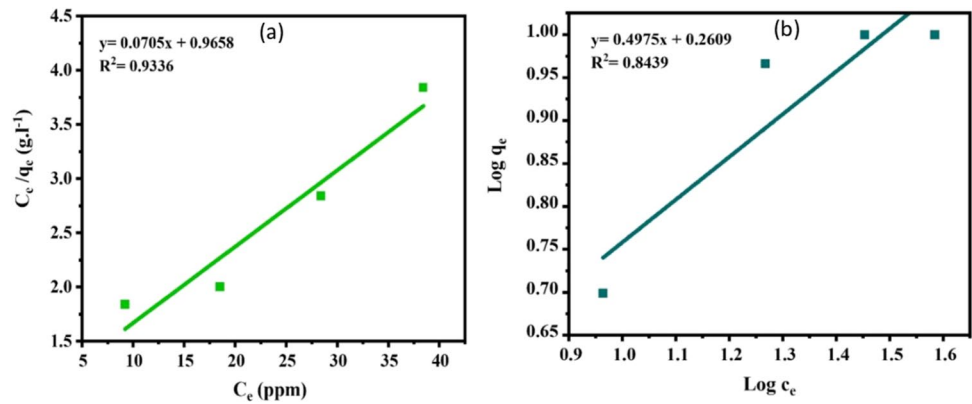**Fig. 8** Linearization of **a** Langmuir and **b** Freundlich isotherm models

Table 3 Isotherm parameters of AZT adsorption onto PAC/Fe/Ag/Zn nano-absorbent

Model	Parameter	Value
Langmuir	q_m (mg/g)	14.18
	K_L(L/mg)	0.073
	R_L	0.25–0.57
	R^2	0.9336
Freundlich	K_f (mg/g)	1.82
	N	2.01
	R^2	0.8439

Fig. 9 Reusability of PAC/Fe/Ag/Zn nano-adsorbent for adsorption removal of AZT antibiotic after 4 cycle adsorption/desorption

Comparing the values of correlation coefficient in the two models of isothermal Langmuir ($R^2 = 0.9336$) and Freundlich ($R^2 = 0.8439$), it is clear that the correlation coefficient in isothermal Langmuir is higher than that of Freundlich and more consistent with the data obtained in the present study. Moreover, the adsorption of AZT on nano-adsorbent PAC/Fe/Ag/Zn is a single layer. The fact that experimental data were more consistent with the Langmuir model is due to the distribution of homogenous active sites on the absorbent surface. On the other hand, in the Langmuir model, the values obtained for R_L are between zero and one, which indicates the favorable adsorption removal of AZT on the nanocomposite PAC/Fe/Ag/Zn. Furthermore, the value of the *n* parameter in the Freundlich isotherm (which is greater than 1) indicates that the adsorption removal of AZT with PAC/Fe/Ag/Zn nano-absorbent is appropriate.

The findings of Mahmoud et al. for the enhanced adsorption removal of levofloxacin and ceftriaxone antibiotics from water using a composite of nano-titanium oxide/chitosan/nano-bentonite showed that experimental data followed from Langmuir isotherm (Mahmoud et al., 2020).
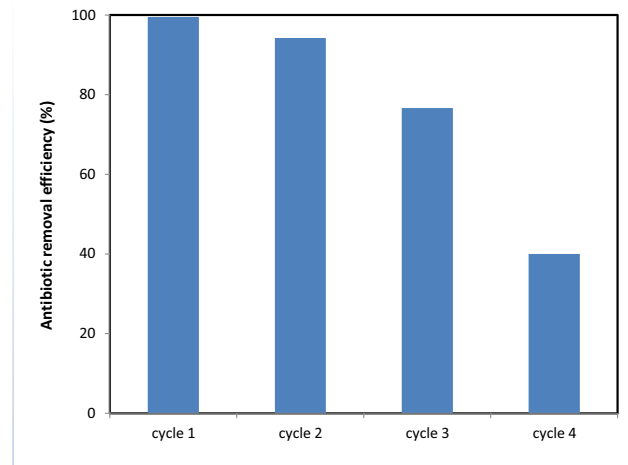
Reuse of PAC/Fe/Ag/Zn nano-adsorbent to remove AZT from aqueous solution

To evaluate the reusability of the AZT, nanoparticles were first collected in the reduction stage during the adsorption removal optimization experiments and used again to remove the antibiotic.

Figure 9 shows the results of reusability experiments of PAC/Fe/Ag/Zn nano-adsorbent after four cycles of use. The results of four replication steps of the adsorption and desorption of the AZT using PAC/Fe/Ag/Zn nano-adsorbents indicate that the adsorption removal rate by PAC/Fe/Ag/Zn nano-adsorbent decreased significantly (from 99.5 to 40%) after four adsorption and desorption cycles. The reason for the decrease in the amount of adsorption may be because most of the adsorption occurs in the surface layers, which are cleared during the desorption steps and are ready to absorb antibiotics again and the depth of the nano-adsorbent pore — which seems to be not completely cleared during the desorption process — is occupied in small amounts by

antibiotic particles. In other words, adsorption and desorption occur mainly in the surface layers of nanoparticles and not in its depths (Song et al., 2019).

Proposed adsorption mechanisms

Different OH-containing groups of AZT to form hydrogen bonding with the surface –Fe, Ag, Zn of PAC/Fe/Ag/Zn nanocomposite are shown in Fig. 10. The tertiary amines in AZT act as a Lewis base to form hydrogen bonding. In addition, the delocalized π-bonds in the N-group had a strong interaction with the π- and σ-electrons of the surface PAC/Fe/Ag/Zn nanocomposite to form conjugate and hyper conjugate structures, respectively. These electron donor–acceptor interactions including the π-π conjugation and σ-π hyperconjugation between the OH and N groups and metal surfaces in PAC/Fe/Ag/Zn nanocomposite may also promote the adsorption of the selected AZT on this composite.

Conclusion

In this study, PAC/Fe/Ag/Zn was successfully synthesized and used as an adsorbent for the removal of AZT antibiotics from the aqueous solutions. The adsorption removal efficiency of AZT by PAC/Fe/Ag/Zn nano-adsorbents from aqueous solution, the 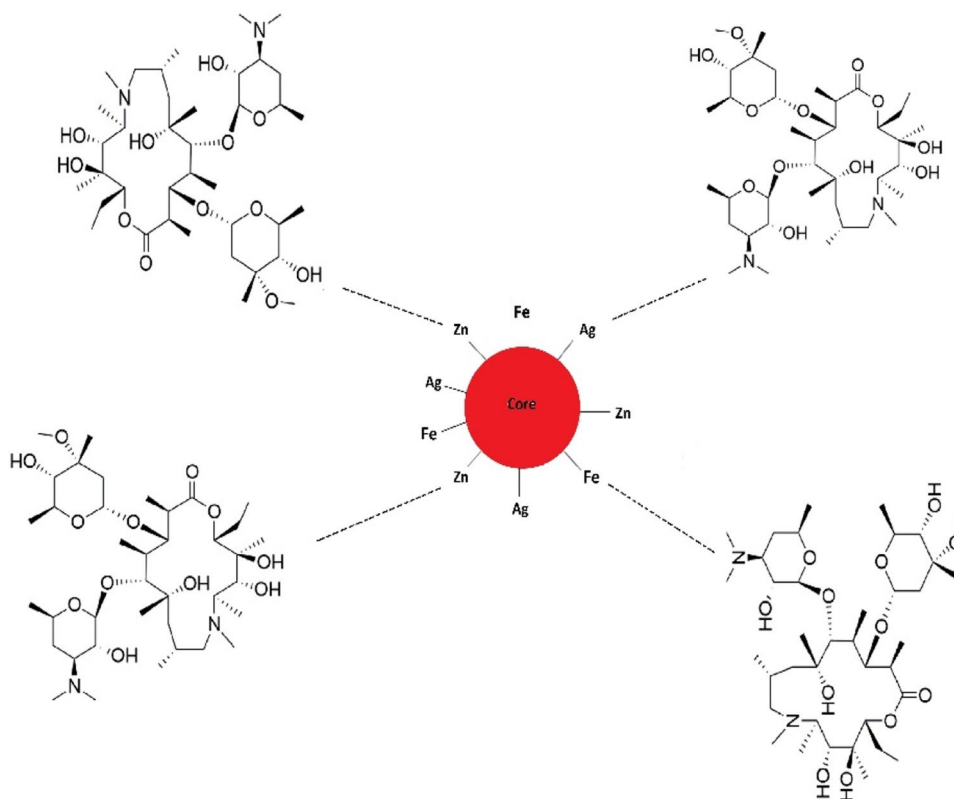impact of effective parameters (pH, contact time, different concentrations of nano-adsorbent, and initial antibiotic concentration), and the determination of optimal parameters were performed.

The removal adsorption of the antibiotic AZT from aqueous solution using PAC/Fe/Ag/Zn nano-adsorbents increased through raising the adsorbent dose and contact time, yet it decreased with raising the initial AZT concentration. Photocatalytic degradation activity was investigated under UV-C irradiation and optimal conditions of pH = 9, 120 min with 0.04 g/l dosage of PAC/Fe/Ag/Zn, and 10 ppm of AZT. The results indicated that 99.5% of AZT was degraded under UV-C irradiation and optimal conditions.

The adsorption isotherm analysis showed that the adsorption process of AZT on the studied adsorbent properly follows the Langmuir model with a correlation coefficient of 0.9336. The results of kinetic studies also indicate that the adsorption behavior of AZT per unit time corresponds to the quasi-first-order kinetic model ($R^2 = 0.9826$).

Due to the favorable performance of PAC/Fe/Ag/Zn in the removal of AZT antibiotic, its feasible separation from the aqueous solutions, and the high activity stability after several cycles (four cycles), it can be used as an efficient adsorbent in the treatment of water and wastewater without further need of filtering and centrifugation. Furthermore, it could be used as an alternative to activated carbon.

Fig. 10 Illustration of interaction between PAC/Fe/Ag/Zn nanocomposite and AZT antibiotic

Declarations

Ethics approval and consent to participate The article has been prepared with the cooperation of all authors.

Consent for publication Not applicable.

Conflict of interest The authors declare no competing interests.

References

Ahmadzadeh S, Dolatabadi M (2018) Electrochemical treatment of pharmaceutical wastewater through electrosynthesis of iron hydroxides for practical removal of metronidazole. Chemosphere 212:533–539

Alalwan HA, Mohammed MM, Sultan AJ, Abbas MN, Ibrahim TA, Aljaafari HA, Alminshid AA (2021) Adsorption of methyl green stain from aqueous solutions using non-conventional adsorbent media: Isothermal kinetic and thermodynamic studies. Bioresource Technology Reports 14:100680

Amin MT, Alazba AA, Shafiq M (2021) Nanofibrous membrane of polyacrylonitrile with efficient adsorption capacity for cadmium ions from aqueous solution: isotherm and kinetic studies. Current Applied Physics. https://doi.org/10.1016/j.cap.2021.03.018

Anirudhan TS, Deepa JR (2017) Nano-zinc oxide incorporated graphene oxide/nanocellulose composite for the adsorption and photo catalytic degradation of ciprofloxacin hydrochloride from aqueous solutions. J Colloid Interface Sci 490:343–356

Arbpour A, Dan S, Hashemipour H (2021) Preparation and optimization of novel graphene oxide and adsorption isotherm study of methylene blue. Arabian Journal of Chemistry 14(3):103003

Babas H, Kaichouh G, Khachani M, Karbane ME, Chakir A, Guenbour A, Zarrouk A (2021) Equilibrium and kinetic studies for removal of antiviral sofosbuvir from aqueous solution by adsorption on expanded perlite: Experimental, modelling and optimization. Surfaces and Interfaces 23:100962

Bachmann SAL, Calvete T, Féris LA (2020) Caffeine removal from aqueous media by adsorption: an overview of adsorbents evolution and the kinetic, equilibrium and thermodynamic studies. Science of The Total Environment. https://doi.org/10.1016/j.scitotenv.2020.144229

Bayati F, Mohammadi MK, Yengejeh RJ, Babaei AA (2021) Ag 2 O/GO/TiO 2 composite nanoparticles: synthesis, characterization, and optical studies. J Aust Ceram Soc 57(1):287–293

Belghadr I, Shams Khorramabadi G, Godini H, Almasian M (2015) The removal of the cefixime antibiotic from aqueous solution using an advanced oxidation process (UV/H2O2). Desalin Water Treat 55(4):1068–1075

Beltran FJ, Aguinaco A, García-Araya JF, Oropesa A (2008) Ozone and photocatalytic processes to remove the antibiotic sulfamethoxazole from water. Water Res 42(14):3799–3808

Chen J, Liu YS, Zhang JN, Yang YQ, Hu LX, Yang YY, Ying GG (2017) Removal of antibiotics from piggery wastewater by biological aerated filter system: treatment efficiency and biodegradation kinetics. Biores Technol 238:70–77

Chen Z, Ma W, Lu G, Meng F, Duan S, Zhang Z, Wei L, Pan Y (2019) Adsorption of levofloxacin onto mechanochemistry treated zeolite: Modeling and site energy distribution analysis. Sep Purif Technol 222:30–34

Cheng S, Zhang C, Li J, Pan X, Zhai X, Jiao Y, Qi X (2021) Highly efficient removal of antibiotic from biomedical wastewater using Fenton-like catalyst magnetic pullulan hydrogels. Carbohydrate Polymers 262:117951

Choi KJ, Kim SG, Kim SH (2008) Removal of antibiotics by coagulation and granular activated carbon filtration. J Hazard Mater 151(1):38–43

Chowdhury A, Kumari S, Khan AA, Chandra MR, Hussain S (2021) Activated carbon loaded with Ni-Co-S nanoparticle for superior adsorption capacity of antibiotics and dye from wastewater: kinetics and isotherms. Colloids and Surfaces A: Physicochemical and Engineering Aspects 611:125868

Dorival-Garcia N, Zafra-Gomez A, Navalón A, González J, Vílchez JL (2013) Removal of quinolone antibiotics from wastewaters by sorption and biological degradation in laboratory-scale membrane bioreactors. Sci Total Environ 442:317–328

Dutta M, Dutta NN, Bhattacharya KG (1999) Aqueous phase adsorption of certain beta-lactam antibiotics onto polymeric resins and activated carbon. Sep Purif Technol 16(3):213–224

Ech-Chihbi E, Nahlé A, Salim R, Benhiba F, Moussaif A, El-Hajjaji F, Zarrouk A (2020) Computational, MD simulation, SEM/EDX and experimental studies for understanding adsorption of benzimidazole derivatives as corrosion inhibitors in 1.0 M HCl solution. Journal of Alloys and Compounds 844:155842

El Bekkali C, Bouyarmane H, El Karbane M, Masse S, Saoiabi A, Coradin T, Laghzizil A (2018) Zinc oxide-hydroxyapatite nanocomposite photocatalysts for the degradation of ciprofloxacin and ofloxacin antibiotics. Colloids Surf, A 539:364–370

Elessawy NA, Elnouby M, Gouda MH, Hamad HA, Taha NA, Gouda M, Eldin MSM (2020) Ciprofloxacin removal using magnetic fullerene nanocomposite obtained from sustainable PET bottle wastes: adsorption process optimization, kinetics, isotherm, regeneration and recycling studies. Chemosphere 239:124728

Foroughi M, Arezoomand HRS, Rahmani AR, Asgari G, Nematollahi D, Yetilmezsoy K, Samarghandi MR (2017) Electrodegradation of tetracycline using stainless steel net electrodes: screening of main effective parameters and interactions by means of a two-level factorial design. Korean J Chem Eng 34(11):2999–3008

Galedari M, Ghazi MM, Mirmasoomi SR (2019) Photocatalytic process for the tetracycline removal under visible light: presenting a degradation model and optimization using response surface methodology (RSM). Chem Eng Res Des 145:323–333

Gao R, Liu D, Huang Y, Li G (2020) Preparation of diatomite-modified wood ceramics and the adsorption kinetics of tetracycline. Ceram Int 46(12):19799–19806

Gashtasbi F, Yengejeh RJ, Babaei AA (2017) Adsorption of vancomycin antibiotic from aqueous solution using an activated carbon impregnated magnetite composite. Desalin Water Treat 88:286–297

Gashtasbi F, Yengejeh RJ, Babaei AA (2018) Photocatalysis assisted by activated-carbon-impregnated magnetite composite for removal of cephalexin from aqueous solution. Korean J Chem Eng 35(8):1726–1734

Gautam RK, Rawat V, Banerjee S, Sanroman MA, Soni S, Singh SK, Chattopadhyaya MC (2015) Synthesis of bimetallic Fe–Zn

nanoparticles and its application towards adsorptive removal of carcinogenic dye malachite green and Congo red in water. J Mol Liq 212:227–236

Ghaedi M, Rozkhoosh Z, Asfaram A, Mirtamizdoust B, Mahmoudi Z, Bazrafshan AA (2015) Comparative studies on removal of Erythrosine using ZnS and AgOH nanoparticles loaded on activated carbon as adsorbents: Kinetic and isotherm studies of adsorption. Spectrochim Acta Part A Mol Biomol Spectrosc 138:176–186

Gholamiyan S, Hamzehloo M, Farrokhnia A (2020) RSM optimized adsorptive removal of erythromycin using magnetic activated carbon: adsorption isotherm, kinetic modeling and thermodynamic studies. Sustainable Chemistry and Pharmacy 17:100309

Ghosh G, Hanamoto S, Yamashita N, Huang X, Tanaka H (2016) Antibiotics removal in biological sewage treatment plants. Pollution 2(2):131–139

Hou X, Shi J, Wang N, Wen Z, Sun M, Qu J, Hu Q (2020) Removal of antibiotic tetracycline by metal-organic framework MIL-101 (Cr) loaded nano zero-valent iron. Journal of Molecular Liquids 313:113512

Huízar-Félix AM, Aguilar-Flores C, Martínez-de-la Cruz A, Barandiarán JM, Sepúlveda-Guzmán S, Cruz-Silva R (2019) Removal of tetracycline pollutants by adsorption and magnetic separation using reduced graphene oxide decorated with α-Fe2O3 nanoparticles. Nanomaterials 9(3):313

Hussain S, Kamran M, Khan SA, Shaheen K, Shah Z, Suo H, Ghani U (2021) Adsorption, kinetics and thermodynamics studies of methyl orange dye sequestration through chitosan composites films. Int J Biol Macromol 168:383–394

Jia S, Yang Z, Yang W, Zhang T, Zhang S, Yang X, Wang Y (2016) Removal of Cu (II) and tetracycline using an aromatic rings-functionalized chitosan-based flocculant: enhanced interaction between the flocculant and the antibiotic. Chem Eng J 283:495–503

Kakavandi B, Esrafili A, Mohseni-Bandpi A, Jonidi Jafari A, Rezaei Kalantary R (2014a) Magnetic Fe3O4@ C nanoparticles as adsorbents for removal of amoxicillin from aqueous solution. Water Sci Technol 69(1):147–155

Kakavandi B, Kalantary RR, Farzadkia M, Mahvi AH, Esrafili A, Azari A, Javid AB (2014b) Enhanced chromium (VI) removal using activated carbon modified by zero valent iron and silver bimetallic nanoparticles. J Environ Health Sci Eng 12(1):1–10

Kanani MV, Dhruv D, Rathod HK, Rathod KN, Rajyaguru B, Joshi AD, Pandya DD (2019) Investigations on structural, optical and electrical property of ZnO-CuO core–shell nano-composite. Scripta Mater 165:25–28

Kavitha G, Subhapriya P, Dhanapal V, Dineshkumar G, Venkateswaran V (2021) Dye removal kinetics and adsorption studies of activated carbon derived from the stems of Phyllanthus reticulatus. Materials Today: Proceedings 45(9):7934–7938

Khan EA, Khan TA (2018) Adsorption of methyl red on activated carbon derived from custard apple (Annona squamosa) fruit shell: equilibrium isotherm and kinetic studies. J Mol Liq 249:1195–1211

Košutićb K, Dolar D, Ašperger D, Kunst B (2007) Removal of antibiotics from a model wastewater by RO/NF membranes. Sep Purif Technol 53(3):244–249

Liu H, Wu R, Tian L, Kong Y, Sun Y (2018) Synergetic photocatalytic effect between 1 T@ 2H-MoS2 and plasmon resonance induced by Ag quantum dots. Nanotechnology 29(28):285402

Liu X, Guo X, Liu Y, Lu S, Xi B, Zhang J, Bi B (2019) A review on removing antibiotics and antibiotic resistance genes from wastewater by constructed wetlands: performance and microbial response. Environmental Pollution 254:112996

Mahmoud ME, El-Ghanam AM, Mohamed RHA, Saad SR (2020) Enhanced adsorption of Levofloxacin and Ceftriaxone antibiotics from water by assembled composite of nanotitanium oxide/

chitosan/nano-bentonite. Materials Science and Engineering: C 108:110199

Mehrdoost A, Jalilzadeh Yengejeh R, Mohammadi MK, Babaei AA, Haghighatzadeh A (2021) Comparative analysis of UV-assisted removal of azithromycin and cefixime from aqueous solution using PAC/Fe/Si/Zn Nanocomposite. Journal of Health Sciences & Surveillance System 9(1):39–49

Mohammed AA, Kareem SL (2019) Adsorption of tetracycline fom wastewater by using Pistachio shell coated with ZnO nanoparticles: equilibrium, kinetic and isotherm studies. Alex Eng J 58(3):917–928

Naraginti S, Yu YY, Fang Z, Yong YC (2019) Visible light degradation of macrolide antibiotic azithromycin by novel ZrO2/Ag@ TiO2 nanorod composite: transformation pathways and toxicity evaluation. Process Saf Environ Prot 125:39–49

Nasseh N, Barikbin B, Taghavi L, Nasseri MA (2019) Adsorption of metronidazole antibiotic using a new magnetic nanocomposite from simulated wastewater (isotherm, kinetic and thermodynamic studies). Compos B Eng 159:146–156

Nnadozie EC, Ajibade PA (2021)Isotherm, kinetics, thermodynamics studies and effects of carbonization temperature on adsorption of Indigo Carmine (IC) dye using C. odorata biochar. Chemical Data Collections 33:100673

Pirsaheb M, Moradi S, Shahlaei M, Wang X, Farhadian N (2019) A new composite of nano zero-valent iron encapsulated in carbon dots for oxidative removal of bio-refractory antibiotics from water. J Clean Prod 209:1523–1532

Qin Y, Zhang H, Tong Z, Song Z, Chen N (2017) A facile synthesis of Fe3O4@ SiO2@ ZnO with superior photocatalytic performance of 4-nitrophenol. J Environ Chem Eng 5(3):2207–2213

Ren S, Boo C, Guo N, Wang S, Elimelech M, Wang Y (2018) Photocatalytic reactive ultrafiltration membrane for removal of antibiotic resistant bacteria and antibiotic resistance genes from wastewater effluent. Environ Sci Technol 52(15):8666–8673

Salari H (2019) Facile template-free synthesis of 3D flower-like Bi2WO6/MoO3 nanocomposites with ultra-thin sheets and their associated photocatalytic properties under visible light irradiation. J Photochem Photobiol, A 385:112069. https://doi.org/10.1016/j.jphotochem.2019.112069

Salari H (2020) Facile synthesis of new Z-scheme Bi2WO6/Bi2MoO6 p–n junction photocatalysts with high photocatalytic activity: Structure, kinetics and mechanism approach. Mater Res Bull 131:110979. https://doi.org/10.1016/j.materresbull.2020.110979

Salari H, Hosseini HH (2021) In situ synthesis of visible-light-driven a-MnO2 nanorod/AgBr nanocomposites for increased photoinduced charge separation and enhanced photocatalytic activity. Mater Res Bull 133:111046. https://doi.org/10.1016/j.materresbull.2020.111046

Salari H, Daliri A, Gholami MR (2018) Graphitic carbon nitride/reduced graphene oxide/silver oxide nanostructures with enhanced photocatalytic activity in visible light. Phys Chem Res 6(4):729–740. https://doi.org/10.22036/pcr.2018.137083.1501

Salari H, Erami M, Dokoohaki MH, Zolghadr AR (2021) New insights into adsorption equilibrium of organic pollutant on MnO2 nanorods: Experimental and computational studies. Journal of Molecular Liquids 117016. https://doi.org/10.1016/j.molliq.2021.117016

Samarghandi MR, Al-Musawi TJ, Mohseni-Bandpi A, Zarrabi M (2015) Adsorption of cephalexin from aqueous solution using natural zeolite and zeolite coated with manganese oxide nanoparticles. J Mol Liq 211:431–441

Saremi F, Miroliaei MR, Nejad MS, Sheibani H (2020) Adsorption of tetracycline antibiotic from aqueous solutions onto vitamin B6-upgraded biochar derived from date palm leaves. Journal of Molecular Liquids 318:114126

Sayadi MH, Sobhani S, Shekari H (2019) Photocatalytic degradation of azithromycin using GO@ Fe3O4/ZnO/SnO2 nanocomposites. J Clean Prod 232:127–136

Sharma P, Kumar N, Chauhan R, Singh V, Srivastava VC, Bhatnagar R (2020) Growth of hierarchical ZnO nano flower on large functionalized rGO sheet for superior photocatalytic mineralization of antibiotic. Chemical Engineering Journal 392:123746

Sohrabi N, Mohammadi R, Ghassemzadeh HR, Heris SSS (2021) Equilibrium, kinetic and thermodynamic study of diazinon adsorption from water by clay/GO/Fe3O4: modeling and optimization based on response surface methodology and artificial neural network. Journal of Molecular Liquids 328:115384

Song Y, Ding Y, Wang F, Chen Y, Jiang Y (2019) Construction of nano-composites by enzyme entrapped in mesoporous dendritic silica particles for efficient biocatalytic degradation of antibiotics in wastewater. Chem Eng J 375:121968. https://doi.org/10.1016/j.cej.2019.121968

Sundaram PS, Sangeetha T, Rajakarthihan S, Vijayalaksmi R, Elangovan A, Arivazhagan G (2020) XRD structural studies on cobalt doped zinc oxide nanoparticles synthesized by coprecipitation method: Williamson-Hall and size-strain plot approaches. Physica B: Condensed Matter 595:412342

Velliyan S, Rajendran KV (2021) Study on the effect of Ce3+ doping on structural, morphological and optical properties of CuO nanoparticles synthesized via combustion technique. Physica B: Condensed Matter. https://doi.org/10.1016/j.physb.2021.413015

Verklin RM, Mandell GL (1977) Alteration of effectiveness of antibiotics by anaerobiosis. J Lab Clin Med 89(1):65–71

Wang X, Wang Y, Li D (2013) Degradation of tetracycline in water by ultrasonic irradiation. Water Sci Technol 67(4):715–721

Wang B, Xu X, Tang H, Mao Y, Chen H, Ji F (2020) Highly efficient adsorption of three antibiotics from aqueous solutions using glucose-based mesoporous carbon. Applied Surface Science 528:147048

Xu Z, Song X, Li Y, Li G, Luo W (2019) Removal of antibiotics by sequencing-batch membrane bioreactor for swine wastewater treatment. Sci Total Environ 684:23–30

Yaqubi O, Tai MH, Mitra D, Gerente C, Neoh KG, Wang CH, Andres Y (2021) Adsorptive removal of tetracycline and amoxicillin from aqueous solution by leached carbon black waste and chitosan-carbon composite beads. Journal of Environmental Chemical Engineering 9(1):104988

Zhang W, Wang B, Hao C, Liang Y, Shi H, Ao L, Wang W (2016a) Au/Cu2O Schottky contact heterostructures with enhanced photocatalytic activity in dye decomposition and photoelectrochemical water splitting under visible light irradiation. J Alloy Compd 684:445–452

Zhang X, Guo W, Ngo HH, Wen H, Li N, Wu W (2016b) Performance evaluation of powdered activated carbon for removing 28 types of antibiotics from water. J Environ Manage 172:193–200

Zhu Y, Yang Q, Lu T, Qi W, Zhang H, Wang M, Chen W (2020) Effect of phosphate on the adsorption of antibiotics onto iron oxide minerals: Comparison between tetracycline and ciprofloxacin. Ecotoxicology and Environmental Safety 205:111345